Spectroscopic investigations of Pr^{3+}:$CaWO_4$ at liquid-helium temperatures

Tian-Shu Yang,[1,2,*] Ming-Xu Su,[1,2] Jian-Yin Huang,[1,2] You-Cai Lv,[1,2] Zong-Quan Zhou,[1,2,3,†] Chuan-Feng Li,[1,2,3,‡] and Guang-Can Guo[1,2,3]

[1]*CAS Key Laboratory of Quantum Information, University of Science and Technology of China, Hefei 230026, China*

[2]*CAS Center For Excellence in Quantum Information and Quantum Physics, University of Science and Technology of China, Hefei 230026, China*

[3]*Hefei National Laboratory, University of Science and Technology of China, Hefei 230088, China*

(Received 17 October 2022; accepted 13 January 2023; published 6 February 2023)

Rare-earth ions doped into low nuclear-spin density host crystals provide a promising platform for quantum information storage and processing. Calcium tungstate ($CaWO_4$) is an attractive host crystal because it can be isotopically enriched to provide a nuclear spin free environment. Here, we report a spectroscopic investigation of the optical transitions and hyperfine transitions of praseodymium ($^{141}Pr^{3+}$) doped in $CaWO_4$ at liquid-helium temperatures. The hyperfine structures of the $^3H_4(0)$ and $^1D_2(0)$ states are determined by spectral hole burning. The results indicate that Pr^{3+}:$CaWO_4$ is an appealing candidate for quantum memory in quantum information processing.

DOI: 10.1103/PhysRevA.107.022802

I. INTRODUCTION

Rare-earth ions doped into crystals at liquid-helium temperatures are promising materials for quantum information processing due to their long optical and spin coherence times [1–3]. Recently, remarkable achievements in quantum storage and quantum networking have been obtained with Pr^{3+}-doped Y_2SiO_5 crystals, such as efficient quantum storage [4,5], multiplexed storage in multiple degrees of freedom [6,7], interfacing with a cold atomic gas [8], and entanglement between the two remote quantum memories [9]. Despite these important achievements, the quantum storage lifetime, as determined by the spin coherence lifetime, is limited to several hundred microseconds in Y_2SiO_5 at zero magnetic field [10]. A much longer spin coherence lifetime is required for the practical implementation of quantum repeaters. However, the magnetic field fluctuations caused by the spin-flip of the Y^{3+} ions in Y_2SiO_5 remain the dominant decoherence source [1,11]. Therefore, a host crystal for rare-earth ions, that can provide a nuclear-spin-free environment, is crucial for practical applications [12].

$CaWO_4$ is a non-yttrium-based crystal, in which most nuclei have no spin. Only the ^{183}W isotope of tungsten (with 14% natural abundance and nuclear spin $I = 1/2$) contributes substantially to magnetic field fluctuations in this crystal. By using non-^{183}W isotopes, $CaWO_4$ can be a spin-free host crystal. Recent results have shown that $CaWO_4$ can be a host crystal for Kramers rare-earth ions, such as Er^{3+} [13–18], Yb^{3+} [19], and Ce^{3+} [20], and an electron spin coherence lifetime up to 23 ms has been obtained in $CaWO_4$ [21].

$CaWO_4$ may provide a promising spin environment for Pr^{3+} [12]. However, the coherent spectroscopic properties of Pr^{3+}:$CaWO_4$ at liquid-helium temperatures have not been reported. Only a few absorption and luminescence spectra of Pr^{3+}:$CaWO_4$ have been carried out at much higher temperatures [22,23], which are not suitable for quantum applications due to the limited coherence lifetimes for optical transitions.

To evaluate the possibility of storing and manipulating quantum information in Pr^{3+}:$CaWO_4$, here we implemented a comprehensive spectroscopic investigation of this material at liquid-helium temperatures. We measured the excited-state lifetime and the ground-state lifetime and determined the hyperfine levels of the $^3H_4(0)$ ground state and the $^1D_2(0)$ excited state by spectral hole burning. This study provides the necessary information for implementing spin-wave quantum memories in this material.

This paper is organized as follows. Section II gives the material properties of the samples in this study. In Sec. III, a variety of optical techniques are used to investigate the spectroscopic properties of Pr^{3+}:$CaWO_4$, including the optical transition frequencies, the absorption coefficient, the fluorescence lifetime, the optical coherence lifetime, the hyperfine structures, and the spectral hole lifetime. Section IV concludes the paper.

II. MATERIAL PROPERTIES

Pr^{3+}:$CaWO_4$ crystals used in this study have a doping concentration of 500 ppm and were supplied by SurfaceNet GmbH. $CaWO_4$ is a tetragonal crystal with space group $I4_1/a$. The unit cell parameters of the crystal are $a = b = 0.524$ nm and $c = 1.137$ nm [17,21,23], and the crystal has a fourfold rotational symmetry around the c axis [17,24]. Pr^{3+} ions

*Present address: State Key Laboratory of Quantum Optics and Quantum Optics Devices, Institute of Opto-Electronics, Shanxi University, Taiyuan, 030006, China.

†zq_zhou@ustc.edu.cn

‡cfli@ustc.edu.cn

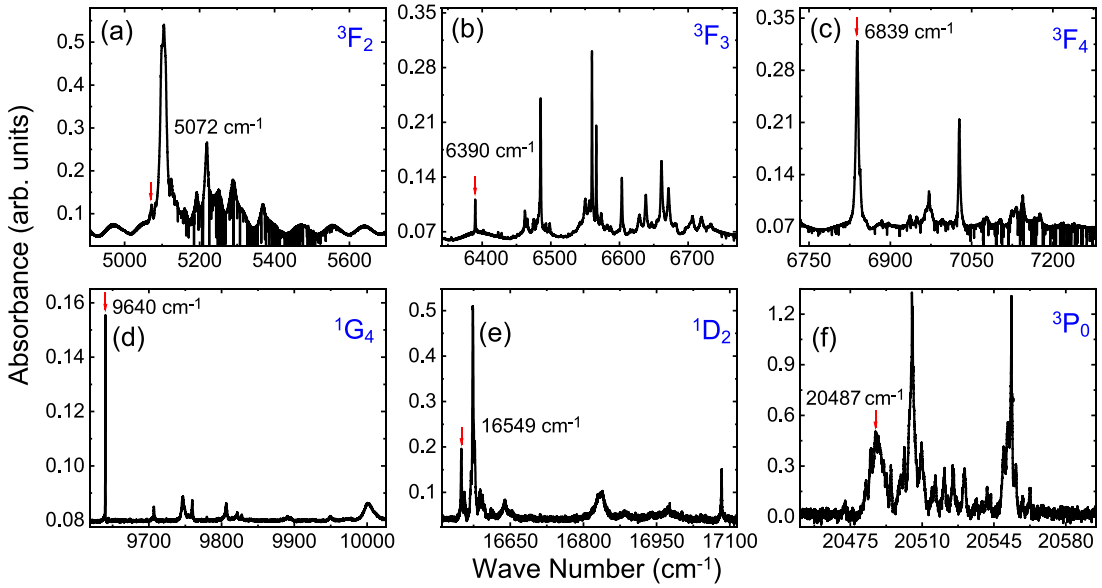

FIG. 1. The FT-IR spectra of Pr^{3+}:$CaWO_4$. The absorption lines from the $^3H_4(0)$ ground state to the $^3F_2$, $^3F_3$, $^3F_4$, $^1G_4$, $^1D_2$, and $^3P_0$ states are shown in panels (a), (b), (c), (d), (e), and (f), respectively. We mark the lowest crystal field level of each state with red arrows and give the wave numbers of these transitions.

substitute Ca^{2+} ions with S_4 point symmetry in $CaWO_4$ crystals. All crystals were cut along the $a \times b \times c$ axes. The $b \times c$ plane was polished, and the light propagated along the a axis.

III. RESULTS AND DISCUSSION

A. Absorption spectra

First, we measured the absorption spectrum to determine the crystal field levels of Pr^{3+}:$CaWO_4$. The absorption spectra of Pr^{3+}:$CaWO_4$ were measured by a Fourier-transform infrared (FT-IR) spectrometer (VERTEX 80, Bruker). The FT-IR spectrum was recorded from the 4000 to 22 000 cm^{-1} wave-number region at a resolution of 0.06 cm^{-1}. Commercial FT-IR spectrometers are operated at room temperature. In this case, Pr^{3+} ions occupy the different crystal field levels and the optical inhomogeneous linewidth is very wide. Pr^{3+} ions only occupy the $^3H_4(0)$ ground state and have a sharp absorption line at liquid-helium temperatures. Therefore, we placed our sample in a cryostat (Cryostation S50, Montana Instruments) with a working temperature of approximately 3.5 K. The FT-IR spectra of Pr^{3+}:$CaWO_4$ were obtained by transmission spectroscopy and the thickness of the crystal was 3 mm.

The absorption spectra for the $^3F_2$, $^3F_3$, $^3F_4$, $^1G_4$, $^1D_2$, and $^3P_0$ manifolds are shown in Fig. 1. These results are in agreement with the previous results reported at 25 K [25]. Here, we got more precise absorption lines at the liquid-helium temperatures. Figure 1 shows that the transition of the lowest crystal field level between the $^3H_4$ state and the $^1D_2$ state is 16 549 cm^{-1} (vacuum wavelength of 604.27 nm), and the full width at half maximum (FWHM) of this transition is 2.57 cm^{-1} (77.1 GHz). This transition can be labeled as $^3H_4(0) \leftrightarrow {}^1D_2(0)$, where 0 refers to the lowest energy levels. Due to the phonon relaxation between the crystal field levels within the multiplets, this transition has a narrow homogeneous linewidth at liquid-helium temperatures [26]. Therefore, this transition is currently most used in Pr^{3+}-based quantum memories [4–9,27].

B. Optical inhomogeneous spectra

In the following, we performed a detailed study of this transition by a continuous-wave laser (TA-SHG Pro, Toptica). First, we scanned the frequency of the laser to obtain the absorption coefficient. The **k** vector of the laser was aligned parallel to the a axis of the crystal and the polarization of the laser was close to the b axis of the crystal.

The result is shown in Fig. 2(a). The absorption center of the transition $^3H_4(0) \leftrightarrow {}^1D_2(0)$ is at 604.25 nm of the vacuum wavelength. The difference between the laser absorption and the FT-IR absorption is due to the difference of the wavelength meter and the FT-IR spectrometer. The optical inhomogeneous linewidth was 85.46 ± 5.56 GHz (FWHM), which was obtained by fitting a Lorentzian line shape. The peak absorption coefficient is $\alpha = 1.877$ cm^{-1} for the Pr^{3+}:$CaWO_4$ crystal.

Then, we investigated the polarization dependence of the absorption coefficient in the $b \times c$ plane. The laser wavelength was set at the absorption center. A half-wave plate was placed in front of the cryostat to adjust the polarization of the input laser. The experimental result is shown in Fig. 2(b).

The dependence of the absorption depth on the polarization angle can be expressed as [28]:

$$I(\phi) = [\cos^2(\phi)e^{-d_\parallel} + \sin^2(\phi)e^{-d_\perp}]I_0 := e^{-d(\phi)}I_0, \quad (1)$$

where ϕ is the polarization angle with respect to the b axis, I_0 is the input intensity, $I(\phi)$ is the output intensity, $d_\parallel$ ($d_\perp$) is the absorption depth for the polarization parallel (perpendicular) to the b axis, and $d(\phi)$ is defined as the effective polarization-dependent absorption depth. The experimental data can be fitted by this formula in Fig. 2(b) (red line). This fit gives

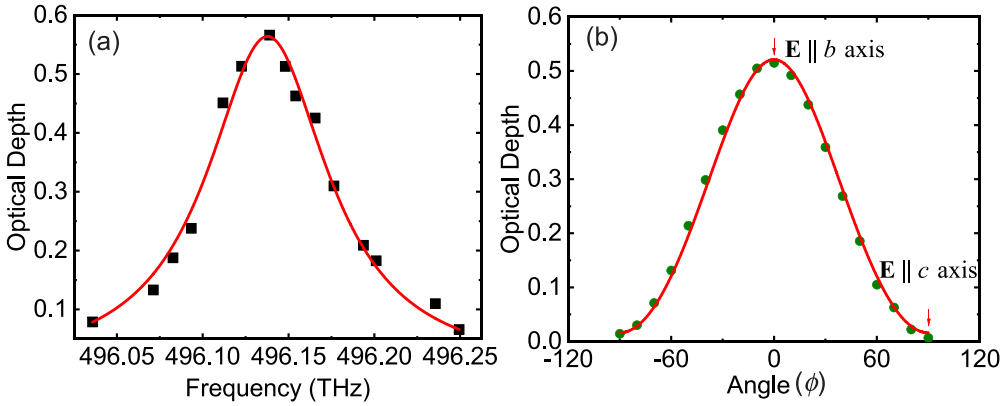

FIG. 2. Absorption spectrum of the transition $^3H_4(0) \leftrightarrow {}^1D_2(0)$ at 604.25 nm (vacuum). (a) The black squares are the measured results, and we fitted them with a Lorentzian line shape (red line). This fit gives the optical inhomogeneous linewidth of 85.46 ± 5.56 GHz. (b) Polarized dependence absorption spectra of Pr^{3+}:$CaWO_4$ for $\mathbf{k} \parallel a$ axis and $\mathbf{E}$ in the b-c plane, where $\mathbf{E}$ is the electric field vector of the laser. The 0° ($\pm 90^\circ$) angle represents that the laser polarization is parallel (perpendicular) to the b axis. The green circles are the measured results, and the red line is fitted by Eq. (1).

$d_\parallel = 0.521 \pm 0.005$ and $d_\perp = 0.016 \pm 0.004$. We found that the strongest absorption for the laser polarized parallel to the b axis. Negligible absorption is observed for the laser polarized perpendicular to the b axis.

C. Fluorescence lifetime of the $^1D_2(0)$ excited state

The population lifetime of the optical excited state gives the upper limit of the optical coherence time T_2 ($T_2 \leqslant 2T_1$). The ratio of the optical T_1 to the ground-state lifetime is important for efficient optical pumping [29].

The $^1D_2(0)$ excited-state fluorescence lifetime was measured by exciting the transition $^3H_4(0) \rightarrow {}^1D_2(0)$ and detecting the transition $^1D_2(0) \rightarrow {}^3H_6$. Four multiphoton single-edge dichroic beam splitters (FF705-Di01-25x36, Semrock) were used as long pass filters to filter out the excitation lasers, and a single-band bandpass filter (FF01-820/12-25, Semrock) was used to filter out the fluorescence from other transitions. We detected the fluorescence by a single-photon detector (SPCM-AQRH-16-FC, Excelitas Technologies). The fluorescence decay curve is shown in Fig. 3(a) with a lifetime T_1 of 56.9 ± 0.2 μs at 3.5 K. This lifetime is similar to those observed for other host crystals, such as Pr^{3+}:$La_2(WO_4)_3$ and Pr^{3+}:$KY(WO_4)_2$ [30,31].

D. Optical coherence measurements

The optical coherence lifetime T_2 limits the quantum storage lifetime in the optical transition. We investigated the optical coherence lifetime of the transition $^3H_4(0) \leftrightarrow {}^1D_2(0)$ using two-pulse photon echo. The photon echo was not observed at 3.5 K. We speculate that this is due to the phonon effect not being sufficiently suppressed, resulting in a short T_2. To further suppress the influence of phonons, we performed the following experiment at 1.7 K (attoDRY2100, Attocube).

To reduce the influence of instantaneous spectral diffusion, we reduced the optical intensity of the excitation pulse. The photon echo was beat with a reference light. The beat signal was detected by a photodetector (Thorlabs, PDA10A) and demodulated by a lock-in amplifier. The excitation pulse was a square wave pulse with a duration of 1 μs. The intensity of the excitation pulse was about 4 W/cm^2.

Figure 3(b) shows the echo amplitude as a function of the delay time. The echo-amplitude decay shows a

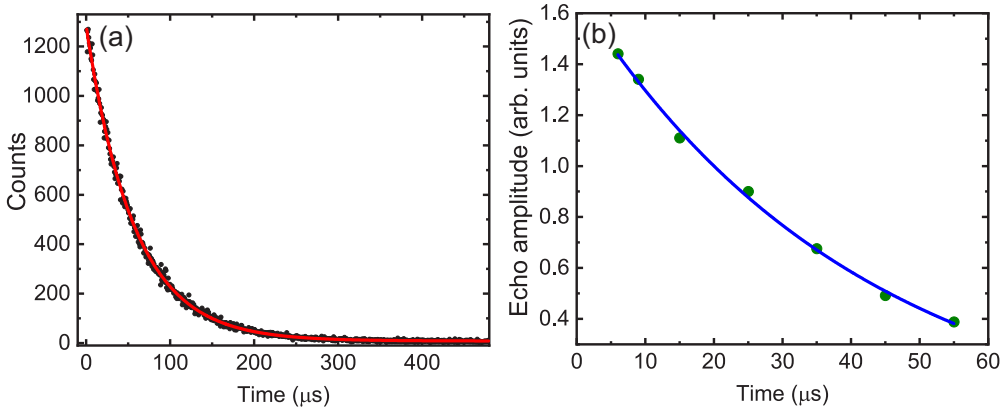

FIG. 3. (a) The $^1D_2(0)$ excited-state lifetime measurement via fluorescence decay at 3.5 K. The black dots are the experimental results. An exponential fit (red line) gives $T_1 = 56.9 \pm 0.2$ μs. (b) Two-pulse photon echo decays of the transition $^1D_2(0) \leftrightarrow {}^3H_4(0)$ at 1.7 K. An exponential fit (blue line) gives $T_2 = 74.2 \pm 6.1$ μs.

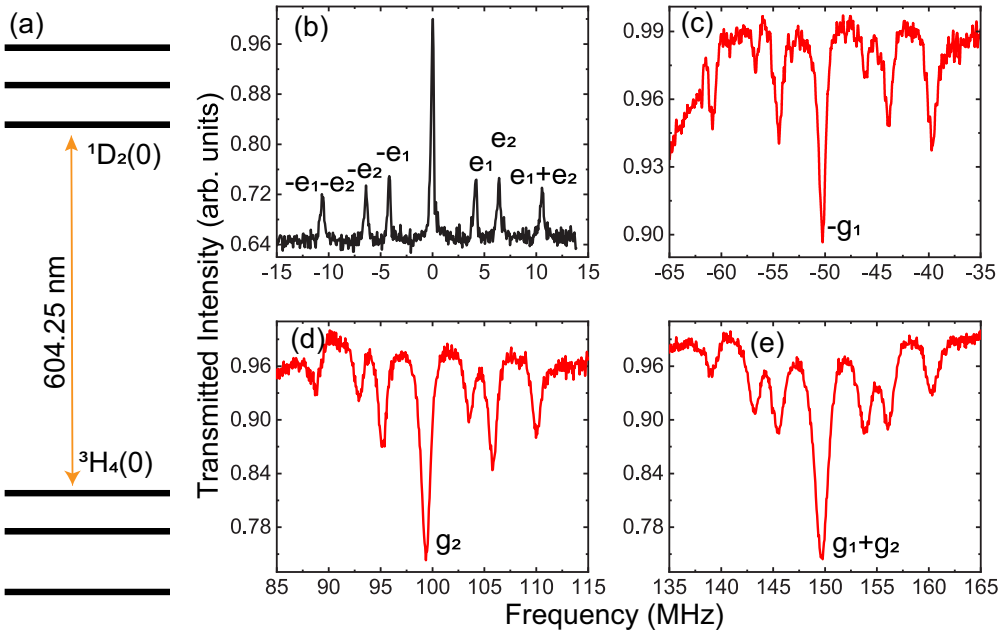

FIG. 4. Hyperfine structures of the $^3H_4(0) \leftrightarrow {}^1D_2(0)$ transition. (a) Hyperfine structures in Pr^{3+}:$CaWO_4$. (b), (c), (d), (e) Experimental results of a single-frequency spectral hole burning. (b) The hole pattern of the spectral hole burning. The side holes are symmetric around the central hole. The side holes are labeled as $-e_1 - e_2$, $-e_2$, $-e_1$, e_1, e_2, and $e_1 + e_2$, where e_1 and e_2 are splittings of the $^1D_2(0)$ excited state. (c), (d), (e) The antihole patterns of spectral hole burning. The antihole positions show that the ground-state hyperfine splittings are 50.3 and 99.3 MHz. We labeled them as g_1 and g_2.

single-exponential character. The coherence time T_2 is 74.2 ± 6.1 μs, corresponding to a homogeneous linewidth of $\Gamma_h = 1/(\pi T_2) = 4.28$ kHz. This homogeneous linewidth is similar to that observed in Pr^{3+}:Y_2SiO_5 [32].

E. Hyperfine structures

For the implementation of the spin-wave atomic frequency combs protocol or the noiseless photon-echo protocol in this crystal [33,34], it is the prerequisite to know the hyperfine structures of the $^3H_4(0)$ ground state and the $^1D_2(0)$ excited state. Pr has a single nuclear isotope (^{141}Pr) and nuclear spin $I = 5/2$. The hyperfine structures of Pr^{3+} consist of three doubly degenerate hyperfine levels in the low site symmetry crystals at zero magnetic field, as shown in Fig. 4(a). The hyperfine structures can be determined by spectral hole burning [35].

Since the optical inhomogeneous linewidth is much larger than the splitting of the hyperfine structures, there are nine classes of ions resonant with a single-frequency laser. Therefore, using a single-frequency laser to burn the crystal, 6 side holes and 42 antiholes can be recorded [35]. The burning pulse was a 1-ms-long single-frequency pulse. The frequency of the probe pulse was scanned by 30 MHz during 400 μs. In the case of antihole measurement, we created a 30-MHz transparent window in the center of the antihole location by sweeping the laser before the spectral hole burning.

The experimental results of the hole and side holes are shown in Fig. 4(b), and the antiholes are shown in Figs. 4(c)–4(e). The $^1D_2(0)$ excited-state splittings 4.2 and 6.4 MHz are obtained from the side-hole positions. The positions of the antiholes reveal that the $^3H_4(0)$ ground-state splittings are 50.3 and 99.3 MHz.

These results are in good agreement with Raman heterodyne detection signals, as shown in Fig. 5. Raman-heterodyne spectra show that the inhomogenous linewidths of these hyperfine transitions are 52.9 ± 0.8 kHz (4.2 MHz), 109 ± 5 kHz (6.4 MHz), 574 ± 6 kHz (50.3 MHz), and 765 ± 16 kHz (99.3 MHz). The large inhomogeneous broadening of hyperfine transitions may indicate that the crystal quality is not good.

Next, we used the dual-frequency hole burning technique to determine the order of ground and excited hyperfine levels [35–37]. We first determined the ordering of the ground-state hyperfine levels. We detected the antiholes at the center frequency of f. Two sets of pump lasers were used: (i) the frequencies of the pump lasers were $f - 50.3$ MHz and $f - 149.6$ MHz, corresponding to the hyperfine levels as shown in Fig. 6(a); and (ii) the frequencies of the pump lasers were $f - 99.3$ MHz and $f - 149.6$ MHz, corresponding to the hyperfine levels as shown in Fig. 6(b). The antiholes at the center frequency of f can be enhanced by the pump lasers at any of these frequencies of $f - 149.6$ MHz, $f - 50.3$ MHz, and $f - 99.3$ MHz. However, the same classes of ions will simultaneously resonate with the correctly ordered pump lasers ($f - 50.3$ MHz/$f - 149.6$ MHz or $f - 99.3$ MHz/$f - 149.6$ MHz). This means that more ions will be pumped to f and around in the correct set of pump lasers. Therefore, in the case of the correct set of pump lasers, the antiholes will be enhanced. Similar analyses can also be found in Refs. [36,37]. The experimental results are shown in Fig. 6(c). One can clearly see that the antiholes in the red (lower) line are enhanced, which indicates that the ordering of

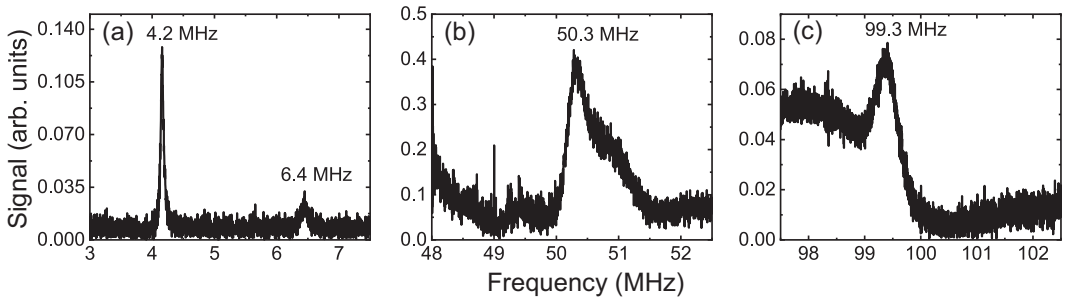

FIG. 5. Raman heterodyne detected hyperfine resonance in Pr^{3+}:$CaWO_4$. (a) Raman heterodyne detected hyperfine resonance of the $^1D_2(0)$ excited-state hyperfine transition. (b), (c) Raman heterodyne detected hyperfine resonance of the $^3H_4(0)$ ground-state hyperfine transition. Due to the frequency response of the Raman heterodyne detection circuit, the regions of the ground-state hyperfine transition have a relatively large noise floor. Furthermore, the large inhomogeneous broadening of hyperfine transitions leads to the resonance peaks being relatively small. These factors lead to the deformation of the resonance profile.

the ground-state hyperfine levels is 50.3 and 99.3 MHz from up to down, as shown in Fig. 6(b).

Then, we began to consider the ordering of the excited-state hyperfine levels. We used two sets of pump lasers ($f - 39.7$ MHz/$f + 103.5$ MHz and $f - 39.7$ MHz/$f + 105.7$ MHz) to burn the crystal. The corresponding hyperfine levels are shown in Figs. 6(d) and 6(e). According to the position of the antiholes, only antiholes at $f - e_1 - e_2$ and f can be enhanced by the pump lasers of $f - 39.7$ MHz, $f + 103.5$ MHz, and $f + 105.7$ MHz. Similar to ground-state ordering analysis, the antiholes at $f - e_1 - e_2$ and f will be enhanced in the case of the correct set of pump lasers. The experimental results are shown in Fig. 6(f). The antiholes in the red (lower in the blue dotted box) line are enhanced, which indicates that the ordering of the excited-state hyperfine levels is 4.2 and 6.4 MHz from up to down. In summary, Fig. 6(e) shows the hyperfine structures of Pr^{3+}:$CaWO_4$ in the $^3H_4(0)$ and $^1D_2(0)$ states.

The effective quadrupole Hamiltonian $H_Q = D(I_z^2 - I(I+1)/3) + E(I_x^2 - I_y^2)$ can be determined by the ground- and

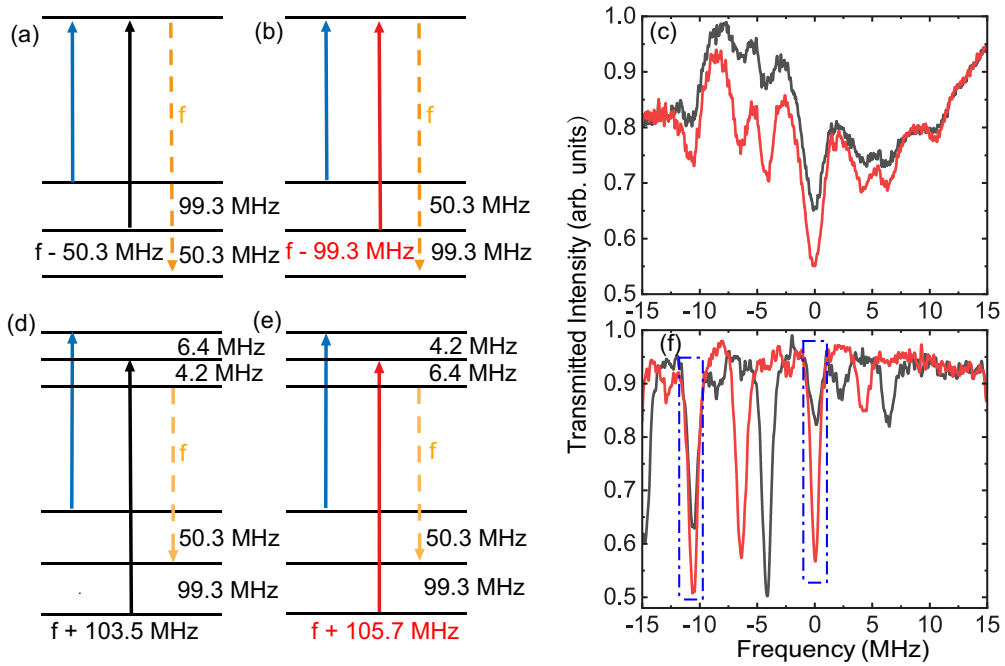

FIG. 6. Dual-frequency hole burning for determining the order of ground- and excited-state hyperfine levels. (a), (b) Two possible ground-state hyperfine levels and two sets of pump lasers. (c) Antiholes of dual-frequency hole burning. The black (upper) line corresponds to the pump set in panel (a), where the pump frequencies are $f - 50.3$ MHz and $f - 149.6$ MHz. The red (lower) line corresponds to the pump set in panel (b), where the pump frequencies are $f - 99.3$ MHz and $f - 149.6$ MHz. Since the red line is enhanced more than the black line, the correct ground-state hyperfine structure is shown in panel (b). (d), (e) Two possible excited-state hyperfine levels and two sets of pump lasers. (f) The black line (upper in the blue dotted box) corresponds to the pump set in panel (d) and the red line (lower in the blue dotted box) corresponds to the pump set in panel (e). Antiholes at -10.6 and 0 MHz, which are marked by blue dotted boxes, will be enhanced by any of these three pump lasers of $f - 39.7$ MHz, $f + 103.5$ MHz, or $f + 105.7$ MHz. Since the red line in the blue dotted boxes is enhanced more than the black line, the correct hyperfine structure is shown in panel (e).

TABLE I. Ground- and excited-state effective quadrupole spin-Hamiltonian parameters (D and E).

Parameter (MHz)	Ground state $^3H_4(0)$	Excited state $^1D_2(0)$
D	13.767	−1.264
E	−12.000	−0.706

excited-state hyperfine structures, where D and E correspond to the combined quadrupole and second-order hyperfine coupling constants in their own principal axes [38]. The fitted D and E of the ground state and the excited state are given in Table I.

F. Spectral hole lifetime

The spectral hole lifetime depends on the time of population redistribution among the three ground-state hyperfine levels and a long spectral hole lifetime is useful for efficient optical pumping [30,39,40].

Here, the spectral hole lifetime was measured by burning a hole in the center of the absorption line and then probing the hole after a variable time. The experimental results are shown in Fig. 7. A single exponential fit of decay gives a lifetime of approximately 0.38 ± 0.02 s at 1.7 K. This value characterizes the effective total lifetime of the hole burning process, since different relaxation rates may occur between different ground-state hyperfine levels. The spectral hole lifetimes could be further extended by lower temperatures, for example, in dilution refrigerators.

IV. CONCLUSIONS

In summary, we investigated the optical inhomogeneous and homogeneous linewidths, the absorption coefficient, the optical population lifetime, the hyperfine structures, and the spectral hole lifetime of Pr^{3+}:$CaWO_4$ at liquid-helium temperatures. The spectral hole lifetime is about 660 times longer than the excited-state lifetime, which is sufficient to perform efficient optical pumping.

We measured an optical coherence time of 74.2 μs, which is sufficient to implement optical quantum memories. The spin coherence time of Pr^{3+} in $CaWO_4$ is another important coherent property. Unfortunately, spin echo was not observed by Raman heterodyne detection. We speculate that this is due to the large spin inhomogeneous linewidth resulting in spin echos too small to be observed. A high-quality single crystal would be useful for further investigations. High-quality crystals may be obtained by annealing treatment to remove crystal defects or optimizing the temperature gradient of the growth furnace to reduce the intrinsic stress [41–43].

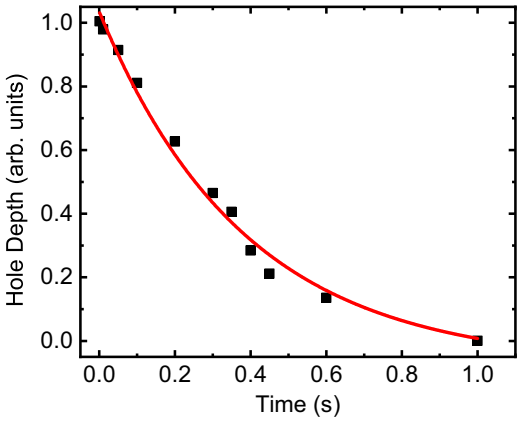

FIG. 7. Decay of the hole depth in Pr^{3+}:$CaWO_4$ at 1.7 K. An exponential fit to the data (red line) gives a hole lifetime of 0.38 ± 0.02 s.

We determined the splitting and the ordering of the $^3H_4(0)$ ground state and the $^1D_2(0)$ excited state by spectral hole burning. These results indicate that Pr^{3+}:$CaWO_4$ is a useful candidate material for quantum interfaces, such as spin-wave quantum memories and integrating with nanophotonic structures to isolate single rare-earth ions [44].

ACKNOWLEDGMENTS

This work is supported by the National Key R&D Program of China (Grant No. 2017YFA0304100), Innovation Program for Quantum Science and Technology (Grant No. 2021ZD0301200), the National Natural Science Foundation of China (Grants No. 12222411, No. 11821404, and No. 62105321), the Fundamental Research Funds for the Central Universities (Grant No. WK2030000046), China Postdoctoral Science Foundation (Grant No. 2021M703111). Z.-Q.Z. acknowledges the support from the Youth Innovation Promotion Association CAS.

[1] M. Zhong, M. P. Hedges, R. L. Ahlefeldt, J. G. Bartholomew, S. E. Beavan, S. M. Wittig, J. J. Longdell, and M. J. Sellars, Optically addressable nuclear spins in a solid with a six-hour coherence time, Nature (London) **517**, 177 (2015).

[2] J. V. Rakonjac, Y.-H. Chen, S. P. Horvath, and J. J. Longdell, Long spin coherence times in the ground state and in an optically excited state of $^{167}Er^{3+}$:Y_2SiO_5 at zero magnetic field, Phys. Rev. B **101**, 184430 (2020).

[3] Y. Ma, Y.-Z. Ma, Z.-Q. Zhou, C.-F. Li, and G.-C. Guo, One-hour coherent optical storage in an atomic frequency comb memory, Nat. Commun. **12**, 2381 (2021).

[4] M. P. Hedges, J. J. Longdell, Y. Li, and M. J. Sellars, Efficient quantum memory for light, Nature (London) **465**, 1052 (2010).

[5] D. Schraft, M. Hain, N. Lorenz, and T. Halfmann, Stopped Light at High Storage Efficiency in a Pr^{3+}:Y_2SiO_5 Crystal, Phys. Rev. Lett. **116**, 073602 (2016).

[6] T.-S. Yang, Z.-Q. Zhou, Y.-L. Hua, X. Liu, Z.-F. Li, P.-Y. Li, Y. Ma, C. Liu, P.-J. Liang, X. Li *et al.*, Multiplexed storage and real-time manipulation based on a multiple degree-of-freedom quantum memory, Nat. Commun. **9**, 3407 (2018).

[7] A. Seri, D. Lago-Rivera, A. Lenhard, G. Corrielli, R. Osellame, M. Mazzera, and H. de Riedmatten, Quantum Storage of Frequency-Multiplexed Heralded Single Photons, Phys. Rev. Lett. **123**, 080502 (2019).

[8] N. Maring, P. Farrera, K. Kutluer, M. Mazzera, G. Heinze, and H. de Riedmatten, Photonic quantum state transfer between a cold atomic gas and a crystal, Nature (London) **551**, 485 (2017).

[9] D. Lago-Rivera, S. Grandi, J. V. Rakonjac, A. Seri, and H. de Riedmatten, Telecom-heralded entanglement between multimode solid-state quantum memories, Nature (London) **594**, 37 (2021).

[10] B. S. Ham, M. S. Shahriar, M. K. Kim, and P. R. Hemmer, Spin coherence excitation and rephasing with optically shelved atoms, Phys. Rev. B **58**, R11825 (1998).

[11] M. Zhong, R. L. Ahlefeldt, and M. J. Sellars, Quantum information processing using frozen core Y^{3+} spins in Eu^{3+}:Y_2SiO_5, New J. Phys. **21**, 033019 (2019).

[12] T. Zhong and P. Goldner, Emerging rare-earth doped material platforms for quantum nanophotonics, Nanophotonics **8**, 2003 (2019).

[13] W. B. Mims, Phase memory in electron spin echoes, lattice relaxation effects in $CaWO_4$: Er, Ce, Mn, Phys. Rev. **168**, 370 (1968).

[14] B. G. Enrique, Optical spectrum and magnetic properties of Er^{3+} in $CaWO_4$, J. Chem. Phys. **55**, 2538 (1971).

[15] S. Bertaina, S. Gambarelli, A. Tkachuk, I. N. Kurkin, B. Malkin, A. Stepanov, and B. Barbara, Rare-earth solid-state qubits, Nat. Nanotechnol. **2**, 39 (2007).

[16] S. Bertaina, J. H. Shim, S. Gambarelli, B. Z. Malkin, and B. Barbara, Spin-Orbit Qubits of Rare-Earth-Metal Ions in Axially Symmetric Crystal Fields, Phys. Rev. Lett. **103**, 226402 (2009).

[17] S. Probst, G. Zhang, M. Rančić, V. Ranjan, M. Le Dantec, Z. Zhang, B. Albanese, A. Doll, R. B. Liu, J. Morton, T. Chanelière, P. Goldner, D. Vion, D. Esteve, and P. Bertet, Hyperfine spectroscopy in a quantum-limited spectrometer, Magn. Reson. **1**, 315 (2020).

[18] M. Rančić, M. L. Dantec, S. Lin, S. Bertaina, T. Chanelière, D. Serrano, P. Goldner, R.-B. Liu, E. Flurin, D. Estève, D. Vion, and P. Bertet, Electron-spin spectral diffusion in an erbium doped crystal at millikelvin temperatures, Phys. Rev. B **106**, 144412 (2022).

[19] R. M. Rakhmatullin, I. N. Kurkin, G. V. Mamin, S. B. Orlinskii, M. R. Gafurov, E. I. Baibekov, B. Z. Malkin, S. Gambarelli, S. Bertaina, and B. Barbara, Coherent spin manipulations in Yb^{3+}:$CaWO_4$ at X- and W-band EPR frequencies, Phys. Rev. B **79**, 172408 (2009).

[20] M. R. Gafurov, I. N. Kurkin, and E. I. Baibekov, Coherence times of Ce^{3+} spin states in $CaWO_4$ crystal, Magn. Reson. Solids **21**, 19501 (2019).

[21] M. Le Dantec, M. Rančić, S. Lin, E. Billaud, V. Ranjan, D. Flanigan, S. Bertaina, T. Chanelière, P. Goldner, A. Erb *et al.*, Twenty-three-millisecond electron spin coherence of erbium ions in a natural-abundance crystal, Sci. Adv. **7**, eabj9786 (2021).

[22] I. Aizenberg, F. Gil'Fanov, and A. Stolov, Absorption and luminescence spectra of Pr^{3+} in $CaWO_4$ monocrystals, Sov. Phys. J. **9**, 29 (1966).

[23] E. Cavalli, P. Boutinaud, and M. Grinberg, Luminescence dynamics in $CaWO_4$:Pr^{3+} powders and single crystals, J. Lumin. **169**, 450 (2016).

[24] C. G. B. Garrett and F. R. Merritt, PMR Spectra of Nd^{3+} in Compensated and Uncompensated $CaWO_4$, Appl. Phys. Lett. **4**, 31 (1964).

[25] C. A. Morrison and R. P. Leavitt, *Spectroscopic properties of triply ionized*, in Handbook on the Physics and Chemistry of Rare Earths (Elsevier, Amsterdam, 1982), pp. 613–616.

[26] C. Thiel, T. Böttger, and R. Cone, Rare-earth-doped materials for applications in quantum information storage and signal processing, J. Lumin. **131**, 353 (2011).

[27] M. Gündoğan, P. M. Ledingham, A. Almasi, M. Cristiani, and H. de Riedmatten, Quantum Storage of a Photonic Polarization Qubit in a Solid, Phys. Rev. Lett. **108**, 190504 (2012).

[28] M. Afzelius, M. U. Staudt, H. de Riedmatten, N. Gisin, O. Guillot-Noël, P. Goldner, R. Marino, P. Porcher, E. Cavalli, and M. Bettinelli, Efficient optical pumping of Zeeman spin levels in Nd^{3+}:YVO_4, J. Lumin. **130**, 1566 (2010).

[29] M. Rančić, M. P. Hedges, R. L. Ahlefeldt, and M. J. Sellars, Coherence time of over a second in a telecom-compatible quantum memory storage material, Nat. Phys. **14**, 50 (2018).

[30] O. Guillot-Noël, P. Goldner, Y. Le Du, P. Loiseau, B. Julsgaard, L. Rippe, and S. Kröll, Hyperfine structure, optical dephasing, and spectral-hole lifetime of single-crystalline Pr^{3+}:$La_2(WO_4)_3$, Phys. Rev. B **75**, 205110 (2007).

[31] H. L. Xu, M. Nilsson, S. Ohser, N. Rauhut, S. Kröll, M. Aguiló, and F. Díaz, Hyperfine structure and homogeneous broadening in Pr^{3+}:$KY(WO_4)_2$, Phys. Rev. B **70**, 214115 (2004).

[32] R. W. Equall, R. L. Cone, and R. M. Macfarlane, Homogeneous broadening and hyperfine structure of optical transitions in Pr^{3+}:Y_2SiO_5, Phys. Rev. B **52**, 3963 (1995).

[33] M. Afzelius, C. Simon, H. de Riedmatten, and N. Gisin, Multimode quantum memory based on atomic frequency combs, Phys. Rev. A **79**, 052329 (2009).

[34] Y.-Z. Ma, M. Jin, D.-L. Chen, Z.-Q. Zhou, C.-F. Li, and G.-C. Guo, Elimination of noise in optically rephased photon echoes, Nat. Commun. **12**, 4378 (2021).

[35] M. Nilsson, L. Rippe, S. Kröll, R. Klieber, and D. Suter, Hole-burning techniques for isolation and study of individual hyperfine transitions in inhomogeneously broadened solids demonstrated in Pr^{3+}:Y_2SiO_5, Phys. Rev. B **70**, 214116 (2004).

[36] B. Lauritzen, N. Timoney, N. Gisin, M. Afzelius, H. de Riedmatten, Y. Sun, R. M. Macfarlane, and R. L. Cone, Spectroscopic investigations of Eu^{3+}:Y_2SiO_5 for quantum memory applications, Phys. Rev. B **85**, 115111 (2012).

[37] M. Jin, Y.-Z. Ma, Z.-Q. Zhou, C.-F. Li, and G.-C. Guo, A faithful solid-state spin-wave quantum memory for polarization qubits, Sci. Bull. **67**, 676 (2022).

[38] R. Macfarlane and R. Shelby, Coherent transient and hole-burning spectroscopy of rare earth ions in solids, in *Modern Problems in Condensed Matter Sciences*, Vol. 21 (Elsevier, Amsterdam, 1987), pp. 51–184.

[39] F. Könz, Y. Sun, C. W. Thiel, R. L. Cone, R. W. Equall, R. L. Hutcheson, and R. M. Macfarlane, Temperature and concentration dependence of optical dephasing, spectral-hole lifetime, and anisotropic absorption in Eu^{3+}:Y_2SiO_5, Phys. Rev. B **68**, 085109 (2003).

[40] R. Klieber, A. Michalowski, R. Neuhaus, and D. Suter, All-optical measurement of nuclear-spin relaxation, Phys. Rev. B **68**, 054426 (2003).

[41] M. Sivers, C. Ciemniak, A. Erb, F. Feilitzsch, A. Gütlein, J.-C. Lanfranchi, J. Lepelmeier, A. Münster, W. Potzel, S. Roth, R. Strauss, U. Thalhammer, S. Wawoczny, M. Willers, and A. Zöller, Influence of annealing on the optical and scintillation properties of $CaWO_4$ single crystals, Opt. Mater. (Amsterdam, Neth.) **34**, 1843 (2012).

[42] A. Erb and J.-C. Lanfranchi, Growth of high-purity scintillating $CaWO_4$ single crystals for the low-temperature direct

dark matter search experiments CRESST-II and EURECA, CrystEngComm **15**, 2301 (2013).

[43] A. Kinast, G. Angloher, G. Benato, A. Bento, A. Bertolini, R. Breier, C. Bucci, L. Canonica, A. D'Addabbo, S. D. Lorenzo, L. Einfalt, A. Erb, F. V. Feilitzsch, N. F. Iachellini, S. Fichtinger, D. Fuchs, A. Fuss, A. Garai, V.-M. Ghete, P. Gorla *et al.*, Improving the quality of $CaWO_4$ target crystals for CRESST, J. Low Temp. Phys. **209**, 1128 (2022).

[44] S. Ourari, L. Dusanowski, S. P. Horvath, M. T. Uysal, C. M. Phenicie, P. Stevenson, M. Raha, S.-H. Chen, R. J. Cava, N. P. de Leon, and J. D. Thompson, Indistinguishable telecom band photons from a single erbium ion in the solid state, arXiv:2301.03564.